Appendix 1 Methods

Participants

A total of 104 participants were recruited in this study, including 73 children with SCP and 31 sex- and age-matched TD children. Patients with SCP were recruited from May 2019 to April 2022 at the Affiliated Hospital of Zunyi Medical University. The inclusion criteria for the patient group were as follows: (I) confirmed diagnosis of SCP by pediatric neurologists; (II) age range from 4 to 14 years old. Exclusion criteria were: (I) conventional MRI showed non-PWMI; (II) poor quality of MRI image or incomplete clinical information. According to these exclusion criteria, 42 children with SCP were excluded (*Figure S1*). During this period, TD children were recruited through the pediatric outpatient department of the hospital. These children were visiting the clinic for minor ailments such as cold and cough. The inclusion criteria of the TD group were: (I) full-term, i.e., 37-42 gestational weeks; (II) age range from 4 to 14 years old; (III) full-Scale intelligence quotient (FSIQ) >70 as assessed by the Wechsler Intelligence Scale for Children; and (IV) no history of neuropsychiatric disorders. Exclusion criteria were poor-quality MRI images or incomplete clinical information. Two TD children were excluded due to poor images. Finally, a total of 60 children (31 SCP and 29 TD) were included for further analyses.

Clinical measurements

All participants underwent intelligence assessment using the Wechsler Intelligence Scale (Chinese version, IV edition), including verbal comprehension index (VCI), working memory index (WMI), processing speed index (PSI), and FSIQ. The children with SCP additionally underwent the Gross Motor Function Classification System (GMFCS) (51), Manual Ability Classification System (MACS) (52), and Communication Function Classification System (CFCS) (53). The GMFCS, MACS, and CFCS were rated from I (good) to V (bad). All clinical assessments, including motor function and cognitive evaluations, were conducted at the time of MRI data collection to ensure that the neuroimaging data corresponded closely with the participants' functional status.

Image acquisition

3D-T1 MRI data were acquired with flip recovery fast spin-echo sequence using a GE Signa HDx 3.0T magnetic resonance scanner for all participants. The imaging parameters were as follows: 146 slices, repetition time =7.8 ms, echo time =3.0 ms, flip angle =15°, field of view =256 mm × 256 mm, matrix =256×256, and slice thickness/gap =1/0 mm. All participants were equipped with noise-canceling earplugs to minimize movement during scanning. Sponges were placed on both sides of their heads to reduce motion artifacts. For uncooperative children, guardians provided informed consent for the use of oral 10% chloral hydrate (0.25-0.5 ml/kg; 10 ml/day at maximum) for sedation during MRI scans.

Data preprocessing

All MRI data were preprocessed using the Computational Anatomy Toolbox (CAT12, http://www.neuro.uni-jena.de/cat) based on Statistical Parametric Mapping software (http://www.fil.ion.ucl.ac.uk/spm/software/spm12/). CAT12 provides a rapid and reliable method for the analysis of surface-based morphometry of the brain, such as CT, fractal dimension (FD), gyrification index (GI), and sulcus depth (SD). First, each structural image was segmented into gray matter, white matter, and cerebrospinal fluid using the study-specific template generated by the Template-O-Matic Toolbox (https://neuro-jena.github.io/software.html#tom). These findings indicate limited effects of the preterm children in the SCP group on the observed between-group differences between the SCP and TD groups. The CT was then estimated and the central surface was reconstructed using the projection-based thickness method. This method allows partial volume information, sulci blurring and sulci asymmetry to be taken into account (54). Based on the constructed central surface, FD, GI, and SD were further calculated using default parameter settings. Finally, individual morphological maps of CT, FD, GI, and SD were re-sampled into the universal fsaverage template and smoothed using a Gaussian kernel with a full width at half maximum of 12 mm for CT and 25 mm for the other morphological measures.

Network construction

First, the multimodal parcellation atlas of the Human Connectome Project (33) was used to parcellate the surface of the cerebral cortex into 360 regions of interest (ROIs), with each ROI representing a node. The regional probability density function was then estimated by kernel

https://dx.doi.org/10.21037/qims-2024-2949

density estimation (MATLAB function: *ksdensity*) for each morphological index by extracting all values within each ROI. The probability density functions were then transformed into the corresponding probability distributions (PDs). The Jensen-Shannon divergence (JSD), a variant of the Kullback-Leibler divergence (KLD), was calculated for two regions with PDs P and Q, respectively, as follows:

$$JSD(P\|Q)=\frac{1}{2}KLD(P\|M)+\frac{1}{2}KLD(Q\|M)$$
$$KLD(P\|Q)=\sum_{i=1}^{n}P(i)\log\frac{P(i)}{Q(i)} \quad [1]$$

where, $M=\frac{1}{2}(P+Q)$ and n is the number of sample points (2^8 in the current study) (55). Finally, the morphological connectivity (MC) between the two regions is defined as:

$$MC_{(P,Q)}=1-\sqrt{JSD(P\|Q)} \quad [2]$$

These procedures generated four sets of 360×360 MC matrices, namely, CT-based networks (CTNs), FD-based networks (FDNs), GI-based networks (GINs), and SD-based networks (SDNs).

Network analysis

Threshold selection

For the MC matrices obtained above, sparsity thresholds are applied to transform each matrix into a set of binary networks, with sparsity defined as the actual number of edges divided by the total number of possible edges in the network. By applying a subject-specific MC threshold to individual MC matrices, the sparsity-based thresholding procedure ensures that the resultant networks have the same number of edges or network cost across all participants. Due to the absence of a definitive method to determine a single sparsity value, the MC matrices were iteratively thresholded over a continuous sparsity range from 0.02 to 0.4 (interval = 0.02). The sparsity range was chosen to ensure that the resulting networks have sparse properties (15,56,57) and can be estimated for small-world attributes (58).

Network measure calculation

In this study, 4 (morphological index: CT/FD/GI/SD) × 20 (sparsity level: 0.02-0.4, interval = 0.02) morphological brain networks were constructed for each participant. For each network, graph-based global (clustering coefficients, C_p, characteristic path length, L_p, normalized C_p, and normalized L_p) and nodal (degree, efficiency, and betweenness) properties were calculated using the GRETNA toolbox (59). Detailed formulas and explanations for these measures can be found elsewhere (41). We further computed the area under the curve for each measure to provide sparsity-independent summary scalars for subsequent statistical analysis since all graph-based network measures are computed as functions or curves of sparsity.

Statistical analysis

Between-group differences in demographic characteristics

The Shapiro-Wilk test was first used to test the normality of age, gestational age, and birth weight. The between-group difference of the categorical variable (sex) was compared using the chi-square test. For each of the remaining quantitative data, an independent-sample *t*-test or a Mann-Whitney *U* test was used to test its between-group difference, depending on whether it followed a normal distribution.

Between-group differences in MRI-based measures

For each morphological index, mean morphological values within each ROI, MC between each ROI pair, and each graph-based network measure were compared between SCP and TD. Briefly, a non-parametric permutation test (10,000 times) was conducted for each variable using the *t* statistic obtained from two-sample *t*-tests. For each intraregional mean morphological value and each nodal property, the false discovery rate (FDR) procedure was used to correct for multiple comparisons between ROIs. For interregional MC, a threshold-free network-based statistics (TFNBS) (60) method was used for the correction of multiple comparisons between connections. Age, sex, weight, and gestational age were considered as covariates in the comparison process.

Relationships between MRI-based measures and clinical variables

For each MRI-based measure showing significant between-group differences, Spearman partial correlations were used to examine its relationships with clinical variables in the SCP, controlling for the effects of sex, age, weight, and gestational age. For correlations between 161 MCs and each clinical variable, an FDR procedure was used to correct for multiple comparisons across all correlation analyses (161 correlation analyses). For correlations between two topological properties and seven clinical variables, an FDR procedure was used to correct for multiple comparisons across all correlation analyses (2×7=14 correlation analyses).

https://dx.doi.org/10.21037/qims-2024-2949

References

51. Palisano RJ, Rosenbaum P, Bartlett D, Livingston MH. Content validity of the expanded and revised Gross Motor Function Classification System. Dev Med Child Neurol 2008;50:744-50.
52. Eliasson AC, Krumlinde-Sundholm L, Rosblad B, Beckung E, Arner M, Ohrvall AM, Rosenbaum P. The Manual Ability Classification System (MACS) for children with cerebral palsy: scale development and evidence of validity and reliability. Dev Med Child Neurol 2006;48:549-54.
53. Hidecker MJC, Paneth N, Rosenbaum PL, Kent RD, Lillie J, Eulenberg JB, Chester Jr KEN, Johnson B, Michalsen L, Evatt M, Taylor K. Developing and validating the Communication Function Classification System for individuals with cerebral palsy. Developmental Medicine & Child Neurology 2011;53:704-10.
54. Dahnke R, Yotter RA, Gaser C. Cortical thickness and central surface estimation. Neuroimage 2013; 65:336-348.
55. Wang H, Jin X, Zhang Y, Wang J. Single-subject morphological brain networks: connectivity mapping, topological characterization and test-retest reliability. Brain Behav 2016;6:e00448.
56. Achard S, Salvador R, Whitcher B, Suckling J, Bullmore E. A resilient, low-frequency, small-world human brain functional network with highly connected association cortical hubs. J Neurosci 2006;26:63-72.
57. Wang J, Wang L, Zang Y, Yang H, Tang H, Gong Q, Chen Z, Zhu C, He Y. Parcellation-dependent small-world brain functional networks: a resting-state fMRI study. Hum Brain Mapp 2009;30:1511-23.
58. Watts DJ, Strogatz SH. Collective dynamics of 'small-world' networks. Nature 1998;393:440-2.
59. Wang J, Wang X, Xia M, Liao X, Evans A, He Y. GRETNA: a graph theoretical network analysis toolbox for imaging connectomics. Front Hum Neurosci 2015;9:386.
60. Baggio HC, Abos A, Segura B, Campabadal A, Garcia-Diaz A, Uribe C, Compta Y, Marti MJ, Valldeoriola F, Junque C. Statistical inference in brain graphs using threshold-free network-based statistics. Hum Brain Mapp 2018;39:2289-302.

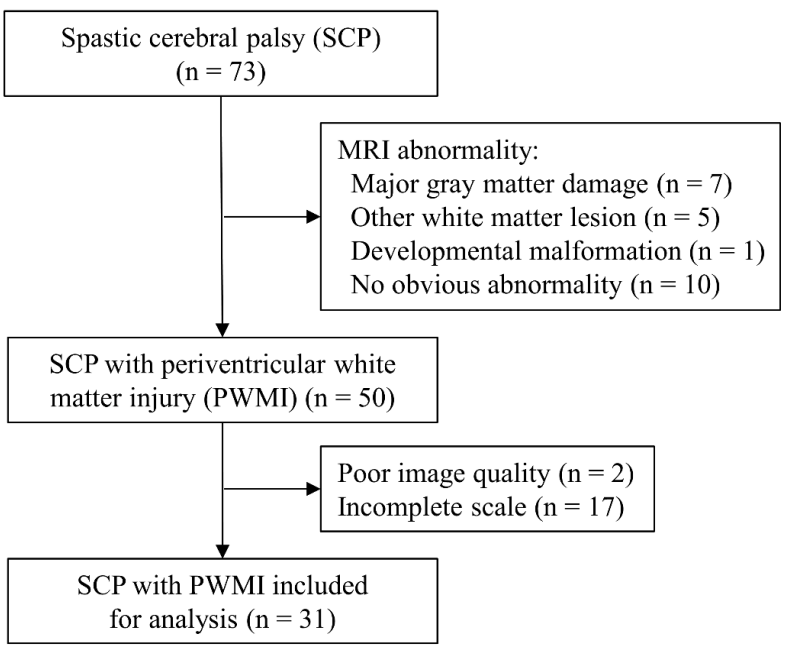

Figure S1 Flow chart of the exclusion process for SCP children with PWMI. SCP, spastic cerebral palsy; PWMI, periventricular white matter injury.

https://dx.doi.org/10.21037/qims-2024-2949